inorganics

MDPI

Article

Mg-Doped Li_2FeTiO_4 as a High-Performance Cathode Material Enabling Fast and Stable Li-ion Storage

Pengqing Hou [1,2], Yingdong Qu [1,*], Rui Huang [2], Xinru Tian [2], Guanglong Li [1] and Shaohua Luo [2,*]

[1] School of Materials Science and Engineering, Shenyang University of Technology, Shenyang 110870, China; 2008hpq@163.com (P.H.); liguanglong1990@163.com (G.L.)
[2] School of Resources and Materials, Northeastern University at Qinhuangdao, Qinhuangdao 066004, China; 18860412701@163.com (R.H.); 15140675197@163.com (X.T.)
* Correspondence: quyingdong@163.com (Y.Q.); tianyanglsh@163.com (S.L.)

Abstract: As a multi-electron system material, the excellent capacity and environmentally benign properties of Li_2FeTiO_4 cathodes make them attractive for lithium-ion batteries. Nevertheless, their electrochemical performance has been hampered by poor conductivity and limited ion transport. In this work, the synthesis of Mg-doped $Li_2Mg_xFe_{1-x}TiO_4$ (LiFT-Mgx, x = 0, 0.01, 0.03, 0.05) cathode materials was successfully achieved. We observed significant gains in interlayer spacing, ionic conductivity, and kinetics. Hence, the sample of the LiFT-Mg0.03 cathode demonstrated charming initial capacity (112.1 mAh g^{-1}, 0.05 C), stability (85.0%, 30 cycles), and rate capability (96.5 mAh g^{-1}, 85.9%). This research provided precious insights into lithium storage with exceptional long-term stability and has the potential to drive the development of next-generation energy storage technologies.

Keywords: Li-ion batteries; Li_2FeTiO_4 cathode; Mg doping; electrochemical performance

1. Introduction

With the development of society, people's demand for fast charging has increased significantly [1–4]. Recently, research on lithium-ion battery cathode materials has shown the advanced nature of keeping pace with the times, and many new materials have slowly entered people's field of vision [5,6]. Li_2FeTiO_4 is typically characterized by high capacity, low cost, non-toxicity and environmental friendliness [7]. In addition, Li_2FeTiO_4 belongs to a multi-electron system, which can realize the transfer of multiple electrons, thus significantly increasing the specific capacity and the energy density of the battery. Based on the advantages of these products, in this era full of environmental awareness, Li_2FeTiO_4 has good appeal. Especially in the field of lithium-ion batteries, this kind of new green and pollution-free material has attracted more and more attention. However, its lack of electrical conductivity and slow dynamic migration seriously damage its practical application value [8]. Carbon coatings are often constructed to improve the dynamics of Li_2FeTiO_4 [9,10]. However, these strategies have been focused on the realization of the surface angle of the material, neglecting to change the internal electric field angle to optimize intrinsic conductivity and ion transport mechanics. Ion doping introduces impurity ions outside the material, causes internal defects, and thus changes the internal electric field distribution or internal carrier concentration of the material, which will improve its intrinsic conductivity and dynamic mobility [11]. Therefore, the study of bulk phase doping design has important practical value and significance for improving the electrochemical properties of Li_2FeTiO_4 materials.

check for updates

Academic Editor: Christian Julien

Received: 18 February 2025
Revised: 3 March 2025
Accepted: 5 March 2025
Published: 6 March 2025

Citation: Hou, P.; Qu, Y.; Huang, R.; Tian, X.; Li, G.; Luo, S. Mg-Doped Li_2FeTiO_4 as a High-Performance Cathode Material Enabling Fast and Stable Li-ion Storage. *Inorganics* **2025**, *13*, 76. https://doi.org/10.3390/inorganics13030076

Copyright: © 2025 by the authors. Licensee MDPI, Basel, Switzerland. This article is an open access article distributed under the terms and conditions of the Creative Commons Attribution (CC BY) license (https://creativecommons.org/licenses/by/4.0/).

In this work, $MgCl_2$ was used as raw material to achieve bulk-phase doping of Mg at the Fe site of Li_2FeTiO_4. Due to the nature of Mg's large ion radius, the extended lithium-ion channel effect was triggered, which ultimately optimized ion migration dynamics. Innovative design of a novel $Li_2Mg_xFe_{1-x}TiO_4$ (LiFT-Mgx, x = 0, 0.01, 0.03, 0.05) cathode material for efficient and stable lithium storage. The mechanism of Mg doping was further discussed. The addition of Mg^{2+} could enlarge the interlayer spacing, promote ion transport, optimize electrode/electrolyte interface conduction, and improve electrochemical kinetics. Electrochemical analysis proved that LiFT-Mg0.03 had a relatively wide ion migration channel and the best charge migration behavior. As a result, the LiFT-Mg0.03 cathode possessed outstanding capacity (112.1 mAh g^{-1}, 0.05 C), stability (85.0%, 30 cycles), and rate performance (96.5 mAh g^{-1}, 85.9%). This research opens up new possibilities for advancing Li_2FeTiO_4 cathode materials aimed at rapid and efficient lithium storage.

2. Results and Discussion

2.1. SEM Analysis of $Li_2Mg_xFe_{1-x}TiO_4$ Samples

SEM was employed to explore the microscopic morphology of the LiFT-Mgx samples. There were no significant changes in the structure (Figure 1a–d). They exhibited a clear calcined body structure, and this was formed by the aggregation of numerous tiny and irregular particles with obvious agglomeration phenomena, and the size of the particles forming the agglomerates ranged from 200 nm to 500 nm. It was declared that Mg doping had little effect on the microscopic morphology of the materials. This phenomenon might be due to the fact that the dopant ions were able to effectively occupy the lattice positions without destroying the symmetry and integrity of the original crystals [12]. Therefore, even if the doped samples showed morphological changes, such as the appearance of new agglomerates or a slight increase or decrease in grain size, these changes were usually localised, controllable and not sufficient to change the overall properties of the material. In addition, these elements (Li, Fe, Ti, Mg, and O) were evenly distributed (Figure 1e). The results confirmed the uniformity and consistent particle size of the synthesized samples, which was crucial for the materials' properties and applications [13].

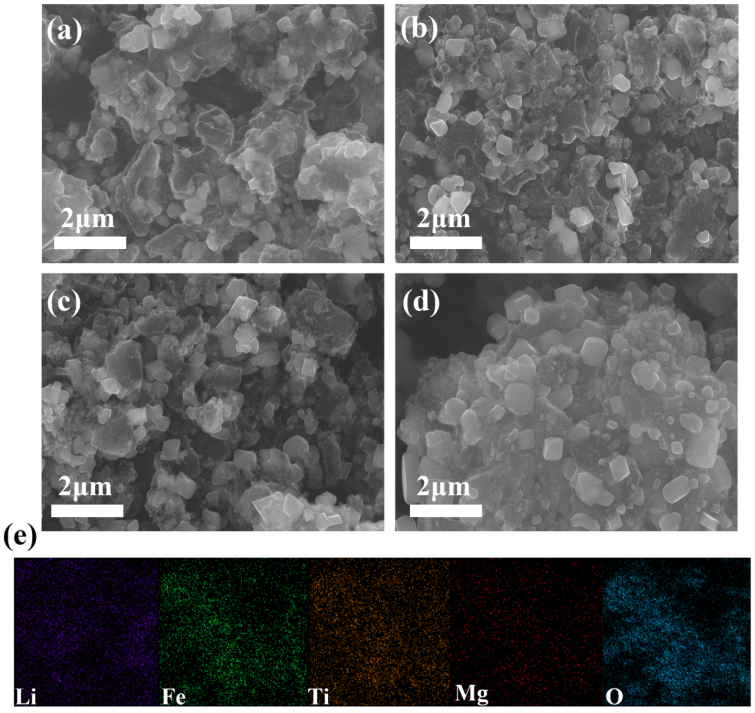


Figure 1. SEM images of: (**a**) LiFT; (**b**) LiFT-Mg0.01; (**c**) LiFT-Mg0.03; (**d**) LiFT-Mg0.05; (**e**) element mapping of LiFT-Mg0.03.

2.2. XRD Analysis of $Li_2Mg_xFe_{1-x}TiO_4$ Samples

In order to further analyse the microstructural morphology as well as the difference in phase species of $Li_2Mg_xFe_{1-x}TiO_4$ materials under different doping levels, XRD plots were compared with each other. According to Figure 2a, it could be seen that the main phase of the sample after Mg doping was still a heterogeneous phase of Li_2FeTiO_4 and Fe_3O_4 [14,15]. Meanwhile, when the doping content reached X = 0.05, the characteristic peaks of Li_2FeTiO_4 gradually became shorter and wider. This might be due to the fact that excessive Mg doping amounts could lead to a decrease in the crystallinity of the sample, ultimately leading to a weakening of the characteristic peak strength [16]. In addition, impurity peaks (Fe_3O_4) existed in the X = 0.05 system. The possible explanation was that excessive doping of Mg^{2+} ions might cause lattice distortion, altering the local charge distribution. This change might prompt the redistribution of Fe^{2+} and Fe^{3+} to form a more stable Fe_3O_4 structure. It was worth noting that LiFT-Mg0.03 was relatively significant in both crystallinity and purity, which meant the most significant ion dynamics. Moreover, it could be seen that with the increase of doping amount, the position of the diffraction peaks shifted towards the direction of small angle corresponding to the arrow (Figure 2b). The (200) peaks exhibited a shift towards higher angles, moving from 43.7° to 43.4°. This suggested that the incorporation of Mg elements led to changes in the interlayer spacing, lattice parameters, and cell volume. This could be due to the larger ionic radius of Mg^{2+} [17]. The increased interlayer spacing in LiFT-Mg0.03 was anticipated to enhance the structure for lithium storage, facilitating faster ion movement and boosting kinetic behavior.

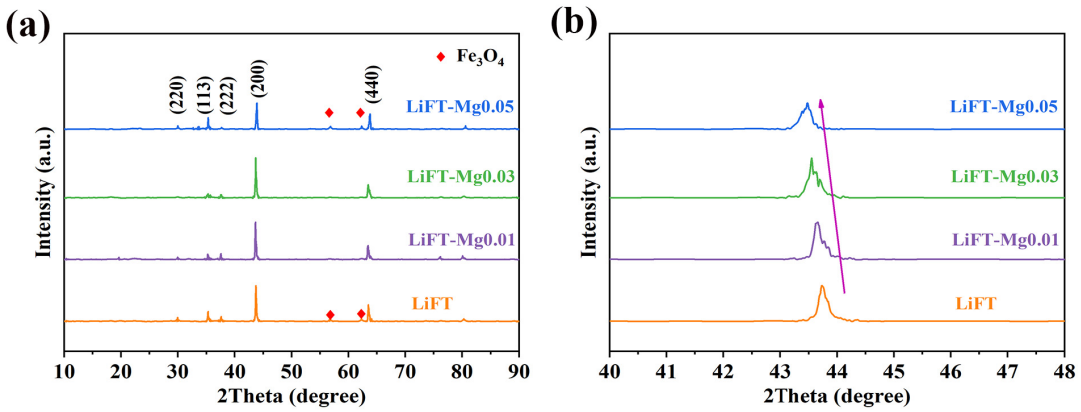


Figure 2. (**a**) XRD images of different samples; (**b**) enlarged images of different samples.

2.3. FTIR Analysis of $Li_2Mg_xFe_{1-x}TiO_4$ Samples

In order to investigate the structure changes of different samples, FTIR was used, as shown in Figure 3. FTIR was performed on the dry gel, pre-fired material, and cathode materials obtained from LiFT-Mg0.03. Peak regions were observed at 860 cm^{-1}, 1000–1600 cm^{-1}, and 3430 cm^{-1}, corresponding to Ti−O, C−O, C−H, and −OH groups, respectively [18]. It could be found that the samples of the three stages were basically similar in terms of peak position, which indicated that the chemical bond had not changed much. However, the strength of the pre-fired samples and the cathode materials in the 1000–1600 cm^{-1} region was weakened because of the decomposition of esters caused by high-temperature calcination.

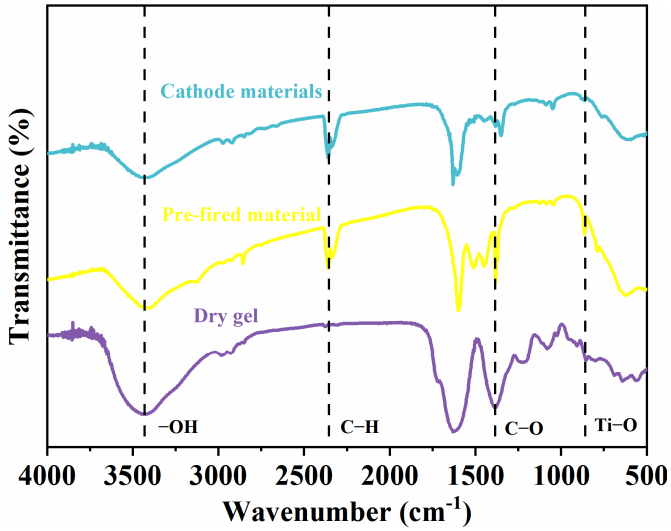


Figure 3. FTIR of LiFT-Mg0.03 at dry gel, pre-fired sample and the cathode material.

2.4. TG-DSC Analysis of $Li_2Mg_xFe_{1-x}TiO_4$ Samples

In order to study the thermal stability of the dry gel of LiFT-Mg0.03 material and its crystallisation process, we decided to carry out TG-DSC analysis (Figure 4). From the figure it can be seen that the whole heating process can be divided into four stages: (1) 25–200 °C; (2) 200–460 °C; (3) 460–680 °C; and (4) 680–1000 °C. In the first stage, about 1.4% of the mass was lost, corresponding to the DSC curve with two absorbing peaks and two exothermic peaks, of which the more obvious absorbing peak at 100 °C corresponded to the loss of water of crystallisation of the compounds; in the second stage, more mass was lost, about 45%, corresponding to the DSC curve with one exothermic peak and two absorbing peaks. One of the absorbing peaks indicated that the thermal decomposition of citric acid occurs to trigger a large amount of weight loss. And the other absorbing peak indicated that the metal salts (e.g., $FeCl_2$, $Ti(OC_4H_9)_4$, CH_3COOLi) had begun to decompose thermally. In the third stage, there was no obvious loss of mass, and the corresponding DSC curve had no obvious heat-absorbing and exothermic peaks. This might be the initial generation of LiFT-Mg0.03 crystals. There was an 8% loss of mass in the fourth stage, and the corresponding DSC curve was relatively flat with no obvious heat-absorbing and exothermic peaks. This stage was the further generation of LiFT-Mg0.03 crystals.

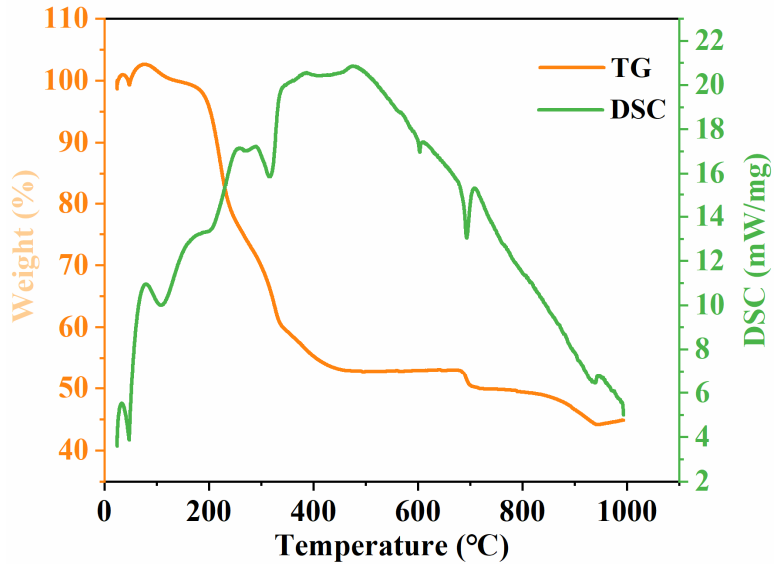


Figure 4. TG-DSC of LiFT-Mg0.03 at dry gel.

2.5. Valence Analysis of $Li_2Mg_xFe_{1-x}TiO_4$ Samples

For further analysis of the elemental valence states of LiFT and the LiFT-Mg0.03 samples, XAS was organized. Standard Fe_2O_3 and FeO reference spectra were used to compare with the K-edge of Fe. Both LiFT and the LiFT-Mg0.03 samples displayed signs of Fe existing in a mixed valence state, with valence states of +2.53 for LiFT and +2.61 for LiFT-Mg0.03 (Figure 5a). This phenomenon indicated that the introduction of Mg^{2+} slightly increased the valence state of the Fe layer, which was conducive to the enhancement of the Fe-O effect and facilitated the rapid migration of lithium ions [19–23]. Additionally, the Ti K-edge XANES spectra revealed that Li_2FeTiO_4 exhibited no notable changes, suggesting that the Ti valence remained consistently at +4 (Figure 5b).

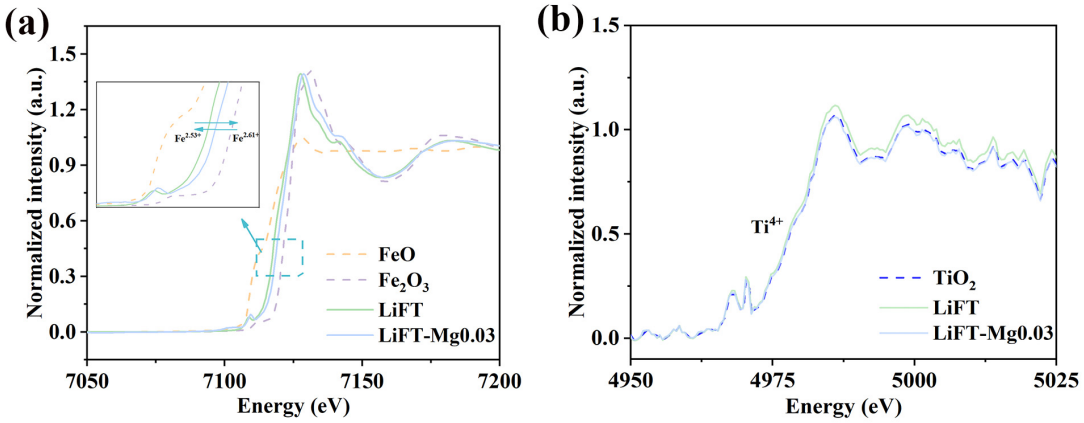


Figure 5. Normalized XAS spectra of: (**a**) Fe K-edge and (**b**) Ti K-edge of LiFT and LiFT-Mg0.03 samples.

2.6. Electrochemical Properties of $Li_2Mg_xFe_{1-x}TiO_4$ Samples

A series of experiments were carried out to examine how Mg doping influences the electrochemical performance of LiFT, including LiFT-Mg0.01, LiFT-Mg0.03, and LiFT-Mg0.05. The initial capacities were measured at 114.5, 113.6, 112.1, and 111.4 mAh g^{-1}, respectively (Figure 6a–d). Because magnesium is chemically inert, its capacity tends to decay as the magnesium content increases. In addition, the repeatability of the charge curves of doped cathode materials was better than that of undoped materials. As a result, Mg doping helped improve structural stability and promoted the fast transport of lithium ions.

In addition, the samples underwent further testing to evaluate their cycling performance at 0.05 C. At the 30th cycle, the capacities of LiFT, LiFT-Mg0.01, LiFT-Mg0.03, and LiFT-Mg0.05 were measured at 79.7, 85.8, 95.3 and 93.4 mAh g^{-1}, representing 69.6%, 75.5%, 85.0% and 83.8% of their initial capacities, respectively (Figure 7a). The LiFT-Mg0.03 cathode material showed the greatest stability across the charge/discharge cycles. Finally, rate performance was evaluated across various current densities (0.05–2.0 C) (Figure 7b). It was observed that as the current density increased, the capacity of all the samples declined. At 2.0 C, the capacities were 56.1, 61.7, 68.1 and 65.4 mAh g^{-1}, which accounted for 48.4%, 54.4%, 60.6% and 58.1% of their initial values, respectively. After cycling the samples back to 0.05 C, the reversible capacities were recorded at 83.5, 88.4, 96.5 and 91.6 mAh g^{-1}, representing 72.0%, 78.0%, 85.9% and 82.4% of the original capacities. Clearly, the LiFT-Mg0.03 cathode material demonstrated the best rate performance, which could be attributed to its wider layer spacing and improved ion transmission characteristics. This finding was further confirmed by XRD and EIS. Moreover, compared with LiFT, LiFT-Mg0.03 had better charge–discharge characteristics at different current densities (Figure 7c,d). The coulomb efficiency of the two samples was greatly improved compared with Figure 6. Because of the pre-activation, the growth of the CEI film was conducive to a more stable charge and discharge.

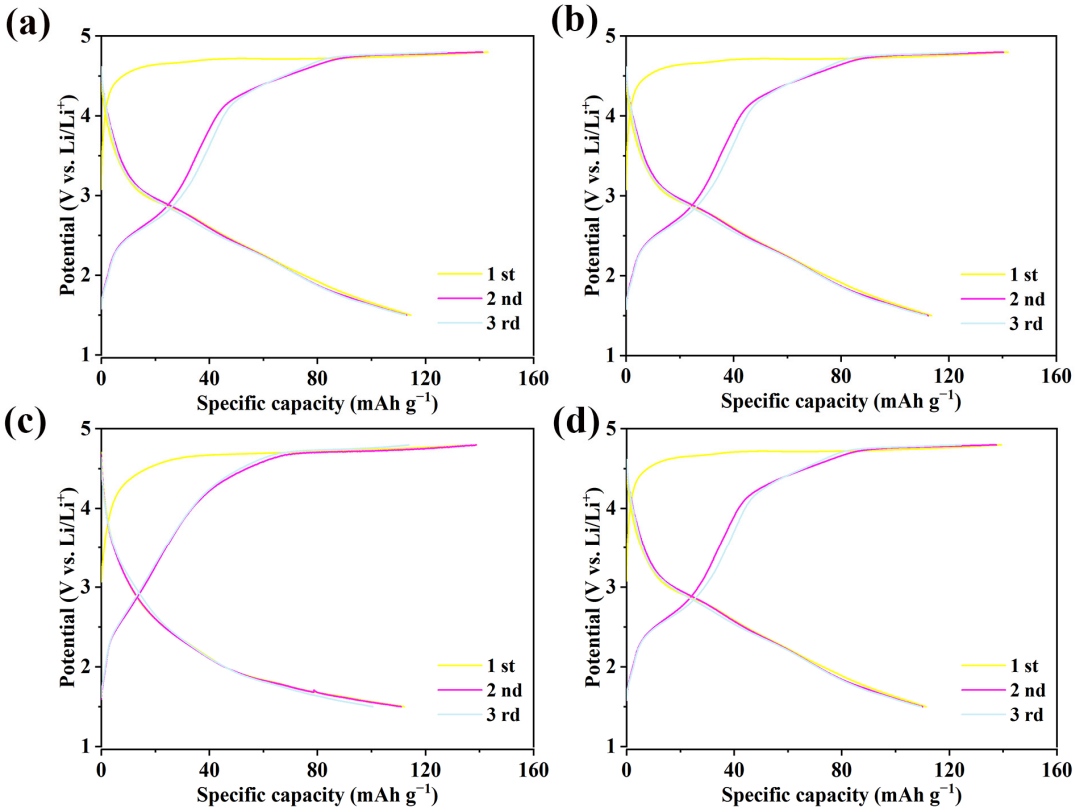


Figure 6. Charge/discharge curves of: (**a**) LiFT; (**b**) LiFT-Mg0.01; (**c**) LiFT-Mg0.03; and (**d**) LiFT-Mg0.05.

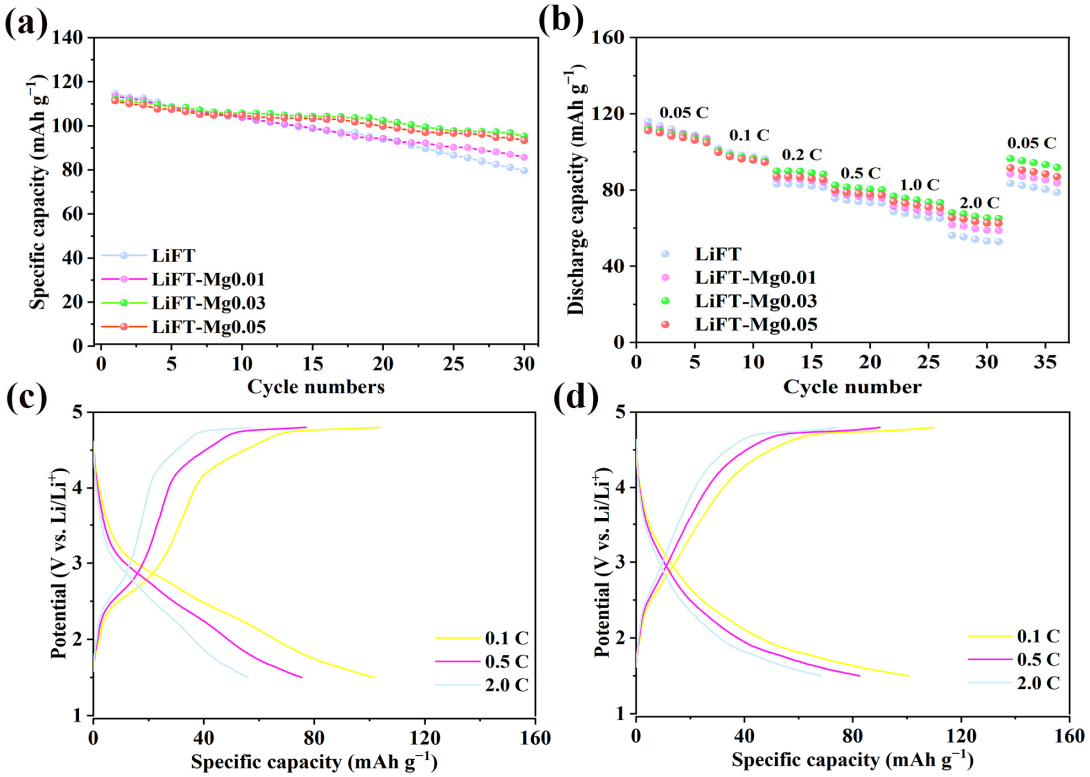


Figure 7. (**a**) Cycle performance; (**b**) rate performance of LiFT, LiFT-Mg0.01, LiFT-Mg0.03, and LiFT-Mg0.05 samples; charge–discharge profiles of (**c**) LiFT and (**d**) LiFT-Mg0.03 samples at varied current densities.

In order to investigate the relationship between impedance and Mg doping, the EIS of different doped materials were compared, as shown in Figure 8. The main features of the

curves were a semicircle and a straight line [24,25]. The high-frequency semicircle was said to be closely related to charge transfer resistance (R_{ct}) and ion migration dynamics [26]. With the increase in doping amount, the impedance of electrode material decreased first and then increased further. The R_{ct} values for LiFT, LiFT-Mg0.01, LiFT-Mg0.03, and LiFT-Mg0.05 were recorded at 1200.8 Ω, 802.5 Ω, 408.8 Ω and 671.9 Ω (Table 1). These results convincingly expounded that Mg doping upgraded the sodium ion movement, and further supported the optimization design of LiFT-Mg0.03.

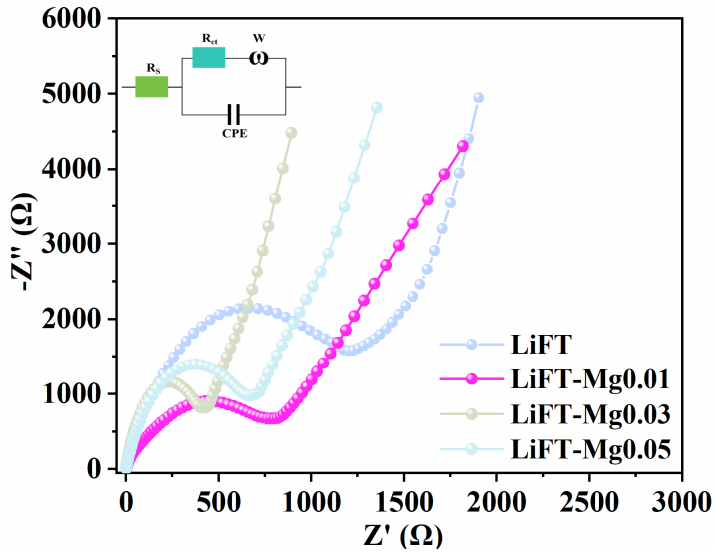


Figure 8. EIS of LiFT, LiFT-Mg0.01, LiFT-Mg0.03, and LiFT-Mg0.05 samples.

Table 1. The fitted impedance (R_s and R_{ct}) for the samples.

	LiFT	LiFT-Mg0.01	LiFT-Mg0.03	LiFT-Mg0.04
R_s (Ω)	8.3	7.4	5.8	6.9
R_{ct} (Ω)	1200.8	802.5	408.8	671.9

In order to better evaluate the effect of a high current environment on LiFT-Mg0.03, we conducted a high current cycle test again. After the study, it was found that LiFT-Mg0.03 still retained 74.4% of the initial value after 200 cycles at 2.0 C (Figure 9a). Then, the morphology and structure of the recycled materials were tested again. After a long cycle, LiFT-Mg0.03 could still maintain its original morphology and crystal structure while the crystallinity decreased after cycling, possibly due to lattice damage caused by long-term charge and discharge (Figure 9b,c). In general, the sample still had the potential for long-term operation with a certain high current.

In order to study the basic history and thermodynamic characteristics of the electrochemical reaction of LiFT-Mg0.03, CV curves were performed at 1.5–4.8 V. It could be noticed that there were still three sets of oxidation peaks and three sets of reduction peaks in Figure 10. And the locations of the peaks in both cycles were strikingly similar, suggesting its favourable electrochemical reversibility. A notable peak appeared in the potential range around 3.0 V, corresponding to the oxidation of Fe^{2+} to Fe^{3+}, a typical reaction observed during cycling [27]. As the voltage increased to 3.8 V, Fe^{3+} was further oxidized to Fe^{4+} [28,29]. These indicated that the battery could store energy reliably while maintaining stability and a long lifespan.

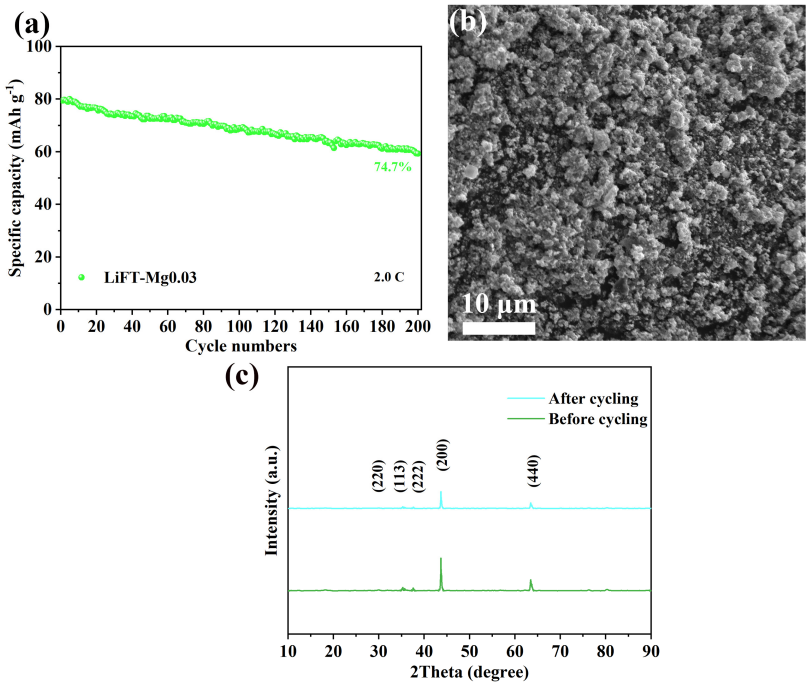


Figure 9. (**a**) Cycle performance at 2.0 C; (**b**,**c**) SEM and XRD of LiFT-Mg0.03 after 200 cycles.

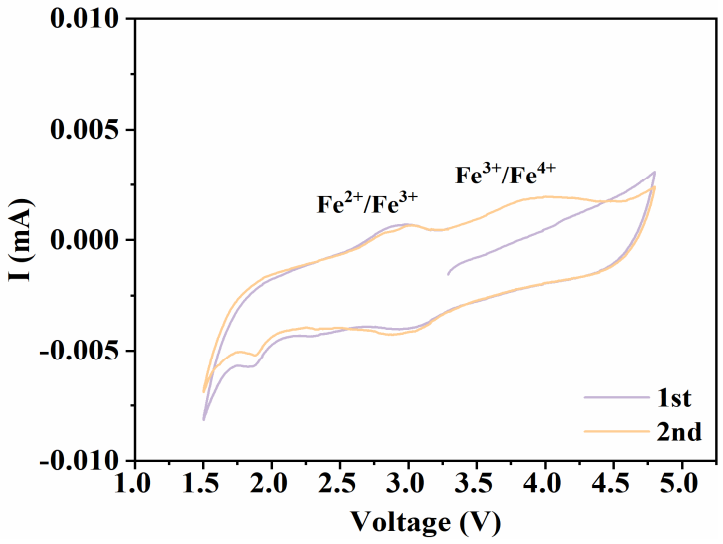


Figure 10. CV curves of LiFT−Mg0.03 material.

3. Materials and Methods

3.1. Material Preparation

The sol–gel technique was employed for creating $Li_2Mg_xFe_{1-x}TiO_4$ (LiFT-Mgx, x = 0, 0.01, 0.03, 0.05). Li, Fe, Ti, and Mg came from $CH_3COOLi{\cdot}2H_2O$, $FeCl_2{\cdot}4H_2O$, tetrabutyl titanate ($Ti(OC_4H_9)_4$), and $MgCl_2{\cdot}6H_2O$, respectively. And citric acid was the chelating agent. The raw materials were initially mixed in ethanol at their stoichiometric ratio. Taking LiFT-Mg0.03 as an example, the molar ratio of $CH_3COOLi{\cdot}2H_2O$, $Ti(OC_4H_9)_4$, $FeCl_2{\cdot}4H_2O$, and $MgCl_2{\cdot}6H_2O$ was 2:1:0.07:0.03. So the amount of $CH_3COOLi{\cdot}2H_2O$, $Ti(OC_4H_9)_4$, $FeCl_2{\cdot}4H_2O$, and $MgCl_2{\cdot}6H_2O$ were 0.2040 g, 0.3403 g, 0.0139 g, and 0.0061 g. And the amount of ethanol was 30 mL. Treating the solution with a water bath (65 °C, 5 h) formed a yellow gel. The gel was then further dried to produce a dry gel (120 °C, 12 h). Next, the high-temperature pretreatment (500 °C, 8 h) in argon was performed on the dry ground gel for the first time. This was the pre-fired sample. Finally, the secondary calcination of the

pre-fired sample was performed at 650 °C for 8 h. Among them, the calcination rate was 5 °C/min, and it was cooled with the furnace.

3.2. Characterization

A scanning electron microscope (SEM Hitachi S-4800, Hitachi, Japan) was suitable for microstructure analysis. The crystal structure was determined using X-ray diffractometry (XRD, Cu-Kα, 5° min^{-1} scan rate, 2θ mode, X/Pert Pro 3040/60), Fourier transform infrared spectroscopy (FTIR, 8400S, Shimadzu, Kyoto, Japan), and Mössbauer spectroscopy (MS, 57Co, Shimadzu). Using X-ray absorption spectroscopy (XAS) at the Beijing Synchrotron Radiation Facility (BSRF)'s beamline 4B9A XRD station, we measured the Ti and Fe K-edges to determine elemental valences.

3.3. Electrochemical Measurements

Synthesized materials, acetylene black, and polyvinylidene fluoride (PVDF) were combined in N-methyl-2-pyrrolidinone (NMP) at an 8:1:1 weight ratio to create the cathode slurry. Subsequently, the cathode slurry was coated on an Al foil, wherein the Al foil was a collector. Following this, it underwent overnight drying at 80 °C. Inside a glovebox, the negative shell, Na sheet, separator, cathode material, gasket, shrapnel and positive shell were assembled in order to obtain the 2032 coin battery. In this group, the electrolyte was lithium iron phosphate (KLD-LFP01), and Celgard 2400 was the separator. Using a LAND system, electrochemical properties were evaluated from 1.5 to 4.8 V.

4. Conclusions

In conclusion, Mg-doped $Li_2Mg_xFe_{1-x}TiO_4$ (LiFT-Mgx, x = 0, 0.01, 0.03, 0.05) cathode materials were synthesized using the sol–gel method. The LiFT-Mg0.03 sample exhibited smaller R_{ct}, indicating superior electrochemical kinetics. As a result, the LiFT-Mg0.03 cathode realized impressive specific capacities (112.1 mAh g^{-1}, 0.05 C) and stability (85.0%, 30 cycles). This could be attributed to the improvement in electrochemical kinetics. This study provided fresh insights into the relationship between structural features and performance, which could open new avenues for the development of advanced Li_2FeTiO_4 cathode materials in future research.

Author Contributions: Conceptualization, P.H. and Y.Q.; methodology, R.H.; software, X.T.; validation, G.L., S.L. and Y.Q.; formal analysis, R.H.; investigation, X.T.; resources, G.L.; data curation, Y.Q.; writing—original draft preparation, P.H.; writing—review and editing, P.H.; visualization, R.H.; supervision, Y.Q.; project administration, S.L.; funding acquisition, Y.Q. All authors have read and agreed to the published version of the manuscript.

Funding: This work was financially supported by the Natural Science Foundation of Hebei Province (E2021501029), and the National Natural Science Foundation of China (52204394).

Data Availability Statement: The original contributions presented in this study are included in the article. Further inquiries can be directed to the corresponding authors.

Conflicts of Interest: The authors declare no competing financial interest.

References

1. Zhang, G.; Zhu, J.; Dai, H.; Wei, X. Multi-level intelligence empowering lithium-ion batteries. *J. Energy Chem.* **2024**, *97*, 535–552. [CrossRef]
2. Wang, J.; Ghosh, T.; Ju, Z.; Ng, M.F.; Wu, G.; Yang, G.; Zhang, X.; Zhang, L.; Handoko, A.D.; Kumar, S.; et al. Heterojunction structure of cobalt sulfide cathodes for high-performance magnesium-ion batteries. *Matter* **2024**, *7*, 1833–1847. [CrossRef]
3. Olutogun, M.; Vanderbruggen, A.; Frey, C.; Rudolph, M.; Bresser, D.; Passerini, S. Recycled graphite for more sustainable lithium-ion batteries. *Carbon Energy* **2024**, *6*, e483. [CrossRef]
4. Ma, H.; Wang, F.; Shen, M.; Tong, Y.; Wang, H.; Hu, H. Advances of $LiCoO_2$ in cathode of aqueous lithium-ion batteries. *Small Methods* **2024**, *8*, 2300820. [CrossRef]

5. Zhao, K.; Yang, Y.; Liu, X.; Wang, Z.L. Triboelectrification-enabled self-charging lithium-ion batteries. *Adv. Energy Mater.* **2017**, *7*, 1700103. [CrossRef]
6. Wu, X.; Liu, Y.; Wang, J.; Tan, Y.; Liang, Z.; Zhou, G. Toward circular energy: Exploring direct regeneration for lithium-ion battery sustainability. *Adv. Mater.* **2024**, *36*, 2403818. [CrossRef]
7. Bruno, S.R.; Blakely, C.K.; Clapham, J.B.; Davis, J.D.; Bi, W.; Alp, E.E.; Poltavets, V.V. Synthesis and electrochemical properties of novel $LiFeTiO_4$ and Li_2FeTiO_4 polymorphs with the $CaFe_2O_4$-type structures. *J. Power Sources* **2015**, *273*, 396–403. [CrossRef]
8. Ma, W.; Tang, Y.; Zhang, Y.; Liu, L.; Tang, B.; Jia, D.; Cao, Y. Cation-disordered Li_2FeTiO_4 nanoparticles with multiple cation and anion redox for symmetric lithium-ion batteries. *Chin. Chem. Lett.* **2024**, 110346, *in press*.
9. Tang, Y.; Liu, L.; Zhao, H.; Zhang, Y.; Kong, L.B.; Gao, S.; Li, X.; Wang, L.; Jia, D. Pseudocapacitive behaviors of Li_2FeTiO_4/C hybrid porous nanotubes for novel lithium-ion battery anodes with superior performances. *ACS Appl. Mater. Interfaces* **2018**, *10*, 20225–20230. [CrossRef]
10. Yang, M.; Zhao, X.; Yao, C.; Kong, Y.; Ma, L.; Shen, X. Nanostructured cation disordered Li_2FeTiO_4/graphene composite as high capacity cathode for lithium-ion batteries. *Mater. Technol.* **2016**, *31*, 537–543. [CrossRef]
11. Wu, Z.; Zhang, C.; Yuan, F.; Lyu, M.; Yang, P.; Zhang, L.; Zhou, M.; Wang, L.; Zhang, S.; Wang, L. Ni-rich cathode materials for stable high-energy lithium-ion batteries. *Nano Energy* **2024**, *126*, 109620. [CrossRef]
12. Liu, Y.; Li, S.; Gu, Z.Y.; Heng, Y.L.; Lu, H.Y.; Yang, J.L.; Du, M.; Wang, X.T.; Guo, J.Z.; Dong, F.; et al. P/S-orbital hybridization induced by Mg-doping to active Na sites in Na_2FePO_4F cathode for long-life and high-rate sodium-ion batteries. *Energy Storage Mater.* **2024**, *68*, 103319. [CrossRef]
13. Kuzma, M.; Dominko, R.; Meden, A.; Makovec, D.; Bele, M.; Jamnik, J.; Gaberšček, M. Electrochemical activity of Li_2FeTiO_4 and Li_2MnTiO_4 as potential active materials for Li ion batteries: A comparison with Li_2NiTiO_4. *J. Power Sources* **2009**, *189*, 81–88. [CrossRef]
14. Chen, R.; Knapp, M.; Yavuz, M.; Ren, S.; Witte, R.; Heinzmann, R.; Hahn, H.; Ehrenberg, H.; Indris, S. Nanoscale spinel $LiFeTiO_4$ for intercalation pseudocapacitive Li^+ storage. *Phys. Chem. Chem. Phys.* **2015**, *17*, 1482–1488. [CrossRef]
15. Ma, W.; Tang, Y.; Zhang, Y.; Li, X.; Liu, L.; Wang, X.; Cao, Y. Synergistic enhancement of ion/electron transport by ultrafine nanoparticles and graphene in Li_2FeTiO_4/C/G nanofibers for symmetric Li-ion batteries. *J. Energy Chem.* **2025**, *101*, 42–51. [CrossRef]
16. Zhao, S.; Yan, K.; Zhang, J.; Sun, B.; Wang, G. Reaction mechanisms of layered lithium-rich cathode materials for high-energy lithium-ion batteries. *Angew. Chem. Int. Ed.* **2021**, *60*, 2208–2220. [CrossRef]
17. Duan, Y.; Ma, Z.H.; Li, L.; Su, G.; Bao, S.; Lu, J.I. Research on sodium storage performance of Cu and Mg doped P2 type layered oxide cathode materials. *J. Electrochem. Soc.* **2024**, *171*, 030502. [CrossRef]
18. Chakrabarti, S.; Thakur, A.K.; Biswas, K. Raman and FTIR spectroscopy study of $LiFeTiO_4$ and Li_2FeTiO_4. *Ionics* **2016**, *22*, 2045–2057. [CrossRef]
19. Dang, R.; Qu, Y.; Ma, Z.; Yu, L.; Duan, L.; Lu, W. The effect of elemental doping on nickel-rich NCM cathode materials of lithium ion batteries. *J. Phys. Chem. C* **2022**, *126*, 151–159. [CrossRef]
20. Qi, M.; Wang, L.; Huang, X.; Ma, M.; He, X. Surface engineering of cathode materials: Enhancing the high performance of lithium-ion batteries. *Small* **2024**, *20*, 2402443. [CrossRef]
21. Chakrabarti, S.; Thakur, A.K.; Biswas, K. Density functional theory study of $LiFeTiO_4$. *J. Power Sources* **2016**, *313*, 81–90. [CrossRef]
22. Cao, Q.; Li, Z.; Cai, L.; Liu, S.; Bu, Z.; Yang, T.; Meng, X.; Xie, R.; Wang, X.; Li, Q.; et al. Voltage control of multiple electrochemical processes during lithium ion migration in $NiFe_2O_4$ ferrite. *ACS Nano* **2024**, *18*, 15261–15269. [CrossRef] [PubMed]
23. Liu, Y.; Chang, C.; Zheng, J. Revealing the role of Mg doping in $LiFe_{0.39}Mg_{0.01}Mn_{0.6}PO_4$/C cathode: Enhanced electrochemical performance from improved electrical conductivity and promoted lithium diffusion kinetics. *J. Energy Storage* **2024**, *91*, 112108. [CrossRef]
24. Chen, S.P.; Lv, D.; Chen, J.; Zhang, Y.H.; Shi, F.N. Review on defects and modification methods of $LiFePO_4$ cathode material for lithium-ion batteries. *Energy Fuels* **2022**, *36*, 1232–1251. [CrossRef]
25. Yang, L.; Luo, S.; Wang, Y.; Zhan, Y.; Wang, Q.; Zhang, Y.; Liu, X.; Mu, W.; Teng, F. Excess capacity on compound phases of Li_2FeTiO_4 composite cathode materials synthesized by hydrothermal reaction using optional titanium sources to boost battery performance. *Chin. Chem. Lett.* **2020**, *31*, 3200–3204. [CrossRef]
26. Dupre, N.; Cuisinier, M.; Zheng, Y.; Fernandez, V.; Hamon, J.; Hirayama, M.; Kanno, R.; Guyomard, D. Evolution of $LiFePO_4$ thin films interphase with electrolyte. *J. Power Sources* **2018**, *382*, 45–55. [CrossRef]
27. Hou, P.; Yang, L.; Wang, Y.; Wang, L.; Li, S.; Luo, S.H. Optimize hydrothermal synthesis and electrochemical performance of Li_2FeTiO_4 composite cathode materials by using orthogonal experimental design method. *Ionics* **2020**, *26*, 1657–1662. [CrossRef]
28. Xu, W.; Zhou, Y.; Ji, X. Lithium-ion-transfer kinetics of single $LiFePO_4$ particles. *J. Phys. Chem. Lett.* **2018**, *9*, 4976–4980. [CrossRef]
29. Yue, J.; Xiong, F.; Shadike, Z.; Gao, X.; Chen, J.; Pi, L.; Yuan, Y.; Qu, B.; Adamson, P.; Ma, L.; et al. A layer-structured high entropy oxide with highly reversible Fe^{3+}/Fe^{4+} redox as advanced cathode material for sodium ion batteries. *J. Power Sources* **2025**, *627*, 235735.

Disclaimer/Publisher's Note: The statements, opinions and data contained in all publications are solely those of the individual author(s) and contributor(s) and not of MDPI and/or the editor(s). MDPI and/or the editor(s) disclaim responsibility for any injury to people or property resulting from any ideas, methods, instructions or products referred to in the content.